PHYSICAL REVIEW D **87,** 115001 (2013)

Concept for a dark matter detector using liquid helium-4

W. Guo*
Mechanical Engineering Department, Florida State University, Tallahassee, Florida 32310, USA

D. N. McKinsey†
Physics Department, Yale University, New Haven, Connecticut 06520, USA
(Received 19 February 2013; revised manuscript received 12 May 2013; published 4 June 2013)

Direct searches for light dark matter particles (mass < 10 GeV) are especially challenging because of the low energies transferred in elastic scattering to typical heavy nuclear targets. We investigate the possibility of using liquid helium-4 as a target material, taking advantage of the favorable kinematic matching of the helium nucleus to light dark matter particles. Monte Carlo simulations are performed to calculate the charge, scintillation, and triplet helium molecule signals produced by recoil He ions, for a variety of energies and electric fields. We show that excellent background rejection might be achieved based on the ratios between different signal channels. The sensitivity of the helium-based detector to light dark matter particles is estimated for various electric fields and light collection efficiencies.

DOI: 10.1103/PhysRevD.87.115001 PACS numbers: 34.50.Gb, 33.50.−j, 82.20.Pm

I. INTRODUCTION

Dark matter, while evident on multiple astronomical length scales through its gravitational effects, has an unknown intrinsic nature. Data from primordial nucleosynthesis [1], the cosmic microwave background [2], structure formation [3], and microlensing observations [4] imply that the dark matter cannot be composed of baryons or active neutrinos, implying new physics beyond the standard model. Experimental direct detection of dark matter particles, illuminating their mass and interaction properties, would therefore create crucial new scientific understanding in both astrophysics and particle physics.

A particularly compelling model for dark matter is that it consists of weakly interacting massive particles, or WIMPs [5,6], with the feature that a massive particle in the early universe interacting through a weak-scale cross section yields a thermal relic abundance approximately that observed for dark matter. Over the past few decades, models of WIMP dark matter have centered on constrained minimal supersymmetry models [7], which predict a stable neutralino with mass greater than 40 GeV, limited to higher masses by the requisite mass difference between the chargino and neutralino. Also, it is commonly argued that in the context of supersymmetry it is most natural for the dark matter mass to be comparable to the weak scale [8,9]. As a result, most direct dark matter experiments have been designed to have excellent sensitivity to dark matter particles with mass comparable to or greater than the weak scale, yet most of these, including the CDMS [10], ZEPLIN [11], and XENON [12,13] programs, see no evidence for such high mass dark matter particles, down to the recent XENON100 spin-independent cross-section limit of about 2×10^{-45} cm^2 at 55 GeV [14]. At the same time, the DAMA [15], CoGeNT [16], and CRESST [17] experiments have seen event rate anomalies that can be interpreted in terms of direct detection of light WIMPs, and a number of astrophysical anomalies may be interpreted in terms of light WIMP annihilation [18]. Meanwhile, many new theories of light WIMPs have been developed, and this is currently an area of active development in particle phenomenology. Models for light dark matter often involve a new mediator particle as well as the dark matter itself, and include the next to minimal supersymmetic model [19], asymmetric dark matter [20], WIMPless dark matter [21], singlet scalars [22], dark sectors with kinetic mixing [23], mirror matter [24]. These models can all evade constraints on light WIMPs from the cosmic microwave background [25], the Large Hadron Collider [26], and Fermi-LAT [27].

Considerable excitement has been generated over the possibility that dark matter particles are relatively low in mass. The difficulty is detecting them, since lighter WIMPs have less kinetic energy and only deposit a small fraction of it when elastically scattering with standard heavy targets like germanium and xenon.

In general it is difficult for heavy targets to be sensitive to light WIMPs, since for typical energy thresholds they are only sensitive to a small part of the WIMP velocity distribution. Models of the WIMP velocity distribution typically assume a Maxwellian distribution of $f(v) = \exp -(v + v_E)^2/v_0^2$, where $v_E \simeq 244$ km/s is the velocity of the Earth around the Milky Way, and $v_0 \simeq 230$ km/s is the virialized velocity of the average particle that is gravitationally bound to the Milky Way [28]. This distribution is expected to be roughly valid up to the Galactic escape velocity $v_{esc} \simeq 544$ km/s, above which the velocity distribution is zero. A plausible energy threshold for Xe, Ge, and He dark matter experiments is about 5 keVnr. But for a

*wguo@magnet.fsu.edu
†daniel.mckinsey@yale.edu

5 GeV WIMP, such as predicted by asymmetric dark matter models [20], its velocity must be particularly large to deposit at least 5 keV. This minimum velocity, $v_{\min}$, is equal to $v_{\min} = \sqrt{\frac{1}{2} \cdot E_R \cdot M_T}/r$, where E_R is the recoil energy, r is the WIMP-target reduced mass $r = M_D \cdot M_T/(M_D + M_T)$, M_D and M_T are the masses of the dark matter particle and the mass of the target nucleus, respectively. For E_R of 5 keV and $M_D = 5$ GeV, $v_{\min}$ is equal to 1127, 864, and 427 km/s for Xe, Ge, and He, respectively. So for this example, $v_{\min}$ is above v_{esc} for Xe and Ge, but not for He. The lower limit of the WIMP-target reduced mass that a detector is sensitive to is given by

$$r_{\text{limit}} = \frac{1}{v_{\text{esc}}} \cdot \sqrt{E_t \cdot M_T/2}, \quad (1)$$

where E_t is the energy threshold. So a kinematic figure of merit for light WIMP detection is the product of the energy threshold and the target mass, which should be minimized for the best light WIMP sensitivity.

This challenge of combined low energy threshold and low target mass can likely be met through the use of liquid helium as a target material. In this paper we investigate the use of liquid helium as a target for light dark matter particles in the mass range of 1 to 10 GeV. In Sec. II we outline the properties of liquid helium in the context of particle detection, and analyze the detectable signals due to scintillation, ionization, and triplet helium molecules produced by low energy WIMP scattering events. In Sec. III we present the results of Monte Carlo simulations to show that excellent discrimination between WIMP scattering events and background electron recoil events may be achieved. In Sec. IV we examine the sensitivity of liquid helium detectors to light WIMPs. We conclude in Sec. V.

II. SIGNALS RESULTING FROM PARTICLE INTERACTIONS IN LIQUID HELIUM

Superfluid helium has been used for a detector material for many applications. Most detector concepts take advantage of the special excitations of the superfluid, and involve detection of phonons, rotons, or quantum turbulence. One example is the HERON concept [29] for pp-solar neutrino detection with rotons in superfluid helium-4 at a temperature of ~100 mK. The HERON researchers also considered using such an instrument to look for dark matter [30,31], with the possibility that the roton/vortex generation by electrons in an applied electric field, combined with prompt roton detection, could be used for particle discrimination. Also, the roton signal could carry information about the nuclear recoil direction. Another is the ULTIMA concept [32] for dark matter detection with quantized turbulence in superfluid helium-3. Both of these concepts have been the subject of considerable research and development in the past few decades.

Along with its many unusual properties related to superfluidity, liquid helium also produces substantial scintillation light and charge when exposed to ionizing radiation, just like liquid xenon and liquid argon which are already used extensively in the search for dark matter. Some ultracold neutron experiments already make use of the prompt scintillation of liquid helium; for example the measurement of the neutron beta-decay lifetime [33] and search for the neutron permanent electric dipole moment at the Spallation Neutron Source [34,35] and the Institute Laue-Langevin [36]. In the development of the neutron electric dipole moment experiments, it has been shown that very high electric fields can be applied to superfluid helium. The prompt scintillation yield in liquid helium is well known, measured by the HERON collaboration to be about 20 photons/keV electron equivalent (keVee).

Depending on particle species, energetic particles elastic scattering in helium can lead to electronic recoils (gamma ray, beta scattering events) or nuclear recoils (neutron or WIMP dark matter scattering events). The recoil electrons or He nucleus collide with helium atoms, producing ionization and excitation of helium atoms along their paths. The ionized electrons can be extracted by an applied electric field. The decay of the helium excimers gives rise to scintillation light. A fraction of the deposited energy is converted into low-energy elementary excitations of the helium, i.e., phonons and rotons. Signals from all these different channels may in principle be used to detect and identify the scattering events.

The key for dark matter detection is to be able to suppress the electronic recoils that make up most of the backgrounds from the nuclear recoils that would make up a WIMP signal by use of event discrimination. In this section, we estimate the nuclear and electronic recoil signals due to ionization charge, prompt scintillation light, metastable He_2^* molecules. For dark matter detection, we want to know how many electrons and scintillation photons we can expect from a nuclear recoil, per keV of recoil energy. Although there are no measurements of these signals from low energy nuclear recoils in helium, fundamental cross section data exist for helium. Therefore we can use those in combination with Lindhard's theory of quenching [37] to estimate the resulting scintillation and charge signals for nuclear recoils. This procedure is likely to be valid considering that the measured yields [38] have been shown to be consistent with Lindhard's theory applied to the total electronic excitation from nuclear recoils in liquid xenon [39].

A. Ionization and scintillation yields of low-energy nuclear recoils in liquid helium

1. Charge state of a recoil He atom

A WIMP dark matter scattering event in liquid helium would result a recoil helium nuclei. Depending on the energy involved in the scattering process, the recoil He can be a bare ion (He^{2+}) or a dressed ion (He^{1+}), or even a

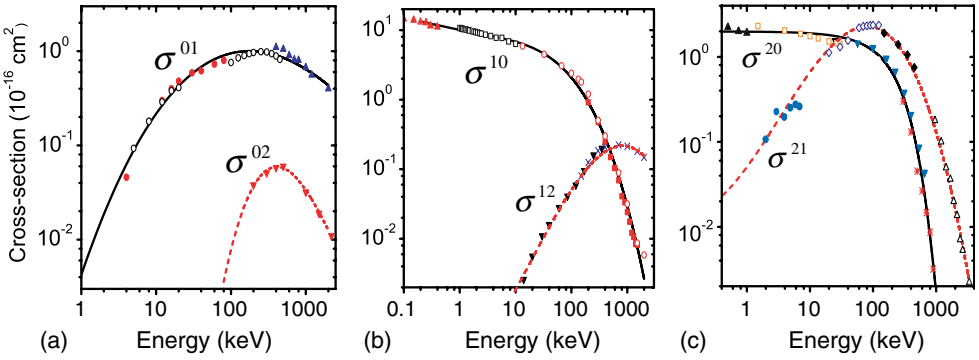

FIG. 1 (color online). Charge exchange cross sections due to He^0, He^{1+}, and He^{2+} interacting with ground state He atoms. The curves were fitted to experimental data by polynomial functions. (a) σ^{01}: solid black line (this work), red (light gray) filled circle (Ref. [87]), black open circle (Ref. [88]), blue (dark gray) filled upward triangle (Ref. [89]); σ^{02}: dashed red line (this work), red (light gray) filled downward triangle (Ref. [89]). (b) σ^{10}: solid black line (this work), red (light gray) filled upward triangle (Ref. [90]), black open square (Ref. [91]), red (light gray) open circle (Ref. [92]), red (light gray) filled square (Ref. [93]); σ^{12}: dashed red line (this work), black filled downward triangle (Ref. [94]), blue (dark gray) crossed symbol (Ref. [92]). (c) σ^{20}: solid black line (this work), black filled upward triangle (Ref. [95]), red (light gray) open square (Ref. [96]), blue (dark gray) filled downward triangle (Ref. [97]), red asterisk symbol (Ref. [98]); σ^{21}: dashed red line (this work), blue (dark gray) filled circle (Ref. [99]), blue (dark gray) open diamond (Ref. [100]), black filled diamond (Ref. [40]), black open triangle (Ref. [101]).

neutral helium atom (He^0). The recoil He dissipates its kinetic energy through collisions with ground state He atoms. Such collisions can be elastic or inelastic that lead to ionization or excitation of He atoms. The ionization and excitation cross sections are different for the recoil He ion in different charge states. As the fast recoil He ion slows down, interactions involving electron capture and loss by the projectile become an increasingly important component of the energy loss process. Charge transfer can produce residual ions without the release of free electrons, and free electrons can be ejected from the moving ion (or neutral) with no residual ions being formed.

Charge transfer cross sections are generally designated as σ^{if} where i represents the initial charge state of the moving ion, and f is the charge state after the collision. For a complete description of the full slowing down of a recoil He, we need cross sections for one-electron capture σ^{21} and two-electron capture σ^{20} for He^{2+}, one-electron capture σ^{10} and one-electron loss σ^{12} for He^{1+}, and one-electron loss σ^{01} and two-electron loss σ^{02} for He^0. In Fig. 1, we show the six charge exchange cross sections based on available experimental data for He^0, He^{1+} and He^{2+}. These cross sections were least-squares fitted by simple polynomial functions of the form $\log(\sigma^{if}) = \sum_n C_n(\log E)^n$, where the C_n's are the fitting parameters, and E is the particle energy in keV. Smooth extrapolation was carried out where the experimental data were l acking. Following the method by Allison [40], the fractions F_0, F_1, and F_2 that the moving particle to be found in charge state 0, 1, and 2 are given by

$$\begin{aligned} dF_0/dz &= N[-F_0(\sigma^{01}+\sigma^{02}) + F_1\sigma^{10} + F_2\sigma^{20}], \\ dF_1/dz &= N[-F_1(\sigma^{10}+\sigma^{12}) + F_0\sigma^{01} + F_2\sigma^{21}], \\ F_2 &= 1 - F_0 - F_1, \end{aligned} \tag{2}$$

where $N \simeq 2.2 \times 10^{22}$ cm^{-3} is the number density of liquid helium and z is the path length along the particle track. If the charge exchange cross sections σ^{if} do not vary as the He ion moves, the equilibrium charge fractions F_0^∞, F_1^∞, and F_2^∞ as $z \to \infty$ are given by Allision [40] as follows:

$$\begin{aligned} F_0^\infty &= (f\sigma^{21} - a\sigma^{20})/D, \\ F_1^\infty &= (b\sigma^{20} - g\sigma^{21})/D, \\ F_2^\infty &= [(a-b)\sigma^{20} + g(a+\sigma^{21}) - f(b+\sigma^{21})]/D, \end{aligned} \tag{3}$$

in which

$$\begin{aligned} a &= -(\sigma^{10}+\sigma^{12}+\sigma^{21}), \qquad b = \sigma^{01} - \sigma^{21}, \\ f &= \sigma^{10} - \sigma^{20}, \qquad g = -(\sigma^{01}+\sigma^{02}+\sigma^{20}), \\ D &= ag - bf. \end{aligned} \tag{4}$$

Figure 2 shows the calculated equilibrium charge fractions as a function of helium ion energy based on

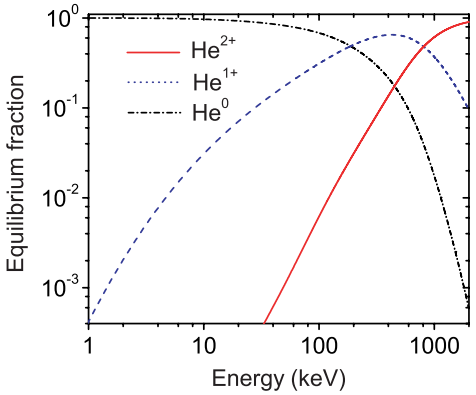

FIG. 2 (color online). Equilibrium fractions of the charge states of an energetic helium ion in liquid helium.

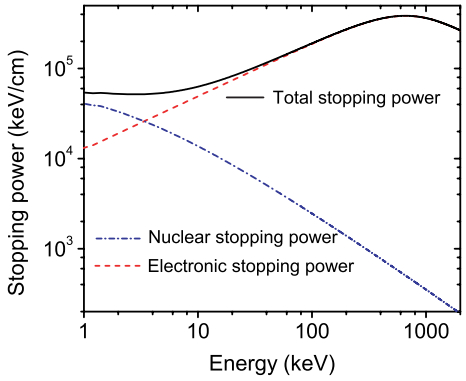

FIG. 3 (color online). Stopping power of a He ion in liquid helium. Data are drawn from the National Institute of Standards and Technology (NIST) database [41].

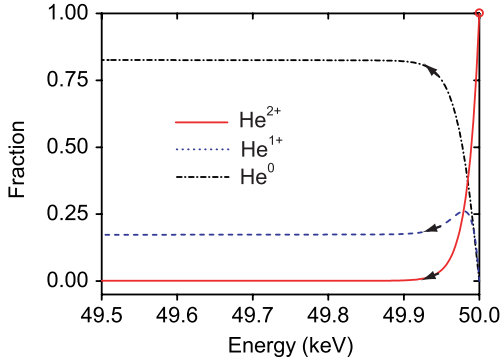

FIG. 4 (color online). Fractions of the charge states of an energetic helium ion as it slows down in liquid helium. The ion started as a He^{2+} with an initial energy of 50 keV, as indicated by the red (light gray) open circle. The arrows show how the fractions evolve as the particle loses its energy.

Eqs. (3) and (4). At energy higher than a few thousands of keV, the helium ion appears primarily as a bare ion He^{2+}, whereas in low energy regime (< 100 keV) the fraction of charge zero state He^0 dominates. The uncertainty in the fits to data in Fig. 1 does not alter this conclusion. To derive these results, it is assumed that σ^{if} does not vary as the He ion moves. In reality, since the charge exchange cross sections depend on particle energy, as a He ion slows down in liquid helium, the σ^{if} in Eq. (2) should change as z varies. In this situation, a full description of variation of the charge fractions F_0, F_1, and F_2 is given by the following equations:

$$\begin{aligned}
\frac{dF_0(E)}{dE} &= \frac{N}{S(E)}[-F_0(\sigma^{01}+\sigma^{02})+F_1\sigma^{10}+F_2\sigma^{20}],\\
\frac{dF_1(E)}{dE} &= \frac{N}{S(E)}[-F_1(\sigma^{10}+\sigma^{12})+F_0\sigma^{01}+F_2\sigma^{21}],\\
F_2(E) &= 1-F_0(E)-F_1(E),
\end{aligned} \tag{5}$$

where $S(E) = dE/dz$ is the total stopping power of a He ion in liquid helium that describes the average energy loss of the He ion per unit path length. $S(E)$ is the sum of the electronic stopping power $S_e(E)$ (energy loss due to the inelastic collisions between bound electrons in the medium and the ion) and the nuclear stopping power $S_n(E)$ (energy loss due to the elastic collisions between the helium atoms and the ion). Figure 3 shows the stopping power data drawn from the National Institute of Standards and Technology (NIST) database [41]. Knowing the stopping power $S(E)$ and the charge exchange cross sections $\sigma^{if}(E)$, one can integrate Eq. (5) to calculate the energy dependence of the fractions of different charge states with a given initial condition. An example is shown in Fig. 4. We see that if we start with a bare ion He^{2+} ($F_2 = 1$) at an initial kinetic energy of 50 keV, as the ion slows down the fractions of the different charge states F_0, F_1, and F_2 quickly evolve to the equilibrium values. This is because that due to the relatively large charge exchange cross sections and the high helium number density, many charge exchange collisions can take place in a short path length of the fast He ion. To achieve the equilibrium charge fractions, only a few charge exchange collisions are needed and the energy loss in this process is small. As a consequence, we can safely use the equilibrium fractions of the charge states to study the slowing down of a fast He ion in liquid helium, with no need to consider the initial charge states.

2. Theoretical analysis of ionization and excitation yields

The ionization and excitation yields due to a recoil helium nuclei moving in liquid helium are important premise parameters needed for the design of a helium-based dark matter detector. Sato *et al.* [42] have studied the ionization and excitation yields of an alpha particle (He^{2+}) in liquid helium using the collision cross sections derived with the binary encounter theory [43]. In their analysis, the charge exchange collisions are ignored and the fraction of the alpha particle energy that is lost to elastic collisions with surrounding He atoms (nuclear stopping) is not included. Nuclear stopping can become dominant when the alpha particle energy is small, which is known as the Lindhard effect [37]. The energy of a recoil helium nuclei in a WIMP scattering event is expected to be relatively low ($\lesssim 100$ keV). To obtain more reliable estimation of the ionization and excitation yields from a recoil helium nuclei, we present an analysis that systematically accounts for both the charge exchange processes and the Lindhard effect.

Assuming a continuous slowing down, the total number of free electrons $N_{\rm el}$ produced along the path of a recoil He nuclei with an initial kinetic energy E is given by

$$\begin{aligned}
N_{\rm el} &= N_{\rm el}^{\rm Dir}+N_{\rm el}^{\rm Exc}+N_{\rm el}^{\rm Sec}\\
&= \int_0^E \frac{N dE'}{S(E')}[F_0^\infty(E')\sigma_{\rm ion}^0+F_{1+}^\infty(E')\sigma_{\rm ion}^{1+}+F_{2+}^\infty(E')\sigma_{\rm ion}^{2+}]\\
&\quad+\int_0^E \frac{N dE'}{S(E')}[F_0^\infty(E')(\sigma^{01}+2\sigma^{02})+F_{1+}^\infty(E')\sigma^{12}]\\
&\quad+N_{\rm ion}^{\rm Sec}.
\end{aligned} \tag{6}$$

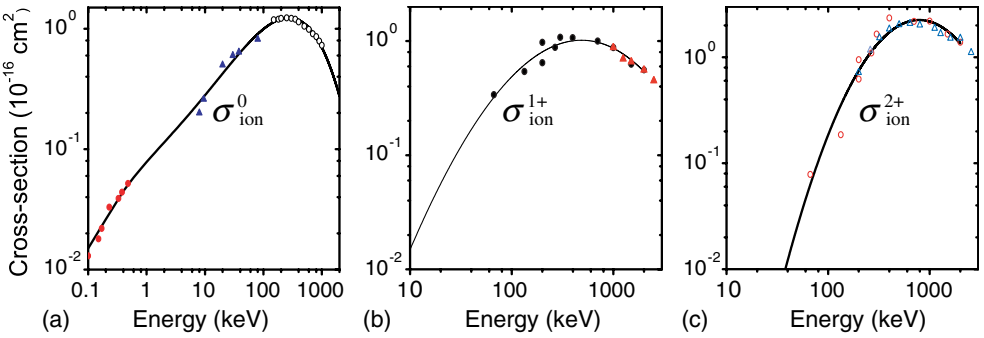

FIG. 5 (color online). Ionization cross sections due to He^0, He^{1+}, and He^{2+} interacting with ground state He atoms. The curves were fitted to experimental data by polynomial functions. (a) σ^0_{ion}: solid black line (this work), red (light gray) filled circle (Ref. [102]), blue (dark gray) filled triangle (Ref. [103]), black open circle (Ref. [104]). (b) σ^{1+}_{ion}: solid black line (this work), black filled circle (Ref. [105]), red (light gray) filled triangle (Ref. [106]). (c) σ^{2+}_{ion}: solid black line (this work), red (light gray) open circle (Ref. [105]), blue (dark gray) open triangle (Ref. [107]).

Here N^{Dir}_{el} and N^{Exc}_{el} are the number of electrons produced in direct ionization and in charge exchange processes due to He ion impact, and are given by the first and the second integral terms on the right side of the equation. σ^0_{ion}, σ^{1+}_{ion}, and σ^{2+}_{ion} are the direct ionization cross sections due to He^0, He^{1+}, and He^{2+} interacting with ground state He atoms, respectively. N^{Sec}_{el} is the number of ionizations produced by secondary electrons that have energy higher than the ionization threshold of a He atom (24.6 eV). F^∞_i $(i = 0, 1, 2)$ is the equilibrium fraction of charge state i as given by Eq. (3). The ratio of N^{Sec}_{el} to N_{el} decreases with decreasing E and is only a few percent when $E \sim 100$ keV [42]. We shall neglect N^{Sec}_{el} in the following analysis for simplicity. To estimate the ionization yield, defined as $Y_{el} = N_{el}/E$, the values of the direct ionization cross sections are needed. In Fig. 5 the experimental data for σ^0_{ion}, σ^{1+}_{ion}, and σ^{2+}_{ion} are shown. We again fit the experimental data by simple polynomial functions $\log(\sigma_{ion}) = \sum_n C'_n (\log E)^n$, and extrapolate the curves where the experimental data were lacking. From Fig. 2 one can see that at $E \lesssim 100$ keV, the fraction of the charge zero state (He^0) dominates. The available ionization and charge exchange cross section data for He^0 in the energy range of 0.1–100 keV allow us to make reliable fit and extrapolation for analyzing the ionization yield. The calculated ionization yield Y_{el} of a recoil He ion as a function of the ion energy is shown in Fig. 6 as the black solid curve.

The total number of excitations N_{ex} produced by a recoil He nuclei with an initial kinetic energy E is given by

$$N_{ex} = \int_0^E \frac{N dE'}{S(E')}[F^\infty_0(E')\sigma^0_{ex} + F^\infty_1(E')\sigma^{1+}_{ex} + F^\infty_2(E')\sigma^{2+}_{ex}] + \tilde{N}_{ex}, \quad (7)$$

where σ^0_{ex}, σ^{1+}_{ex}, and σ^{2+}_{ex} are the total excitation cross sections due to He^0, He^{1+}, and He^{2+} interacting with ground state He atoms, respectively. Here $\tilde{N}_{ex}$ is the number of excitations produced by secondary electrons, which can again be neglected at $E \lesssim 100$ keV [42]. Experimental excitation cross-section data are limited. For instance, Kempter *et al.* estimated the excitation cross sections due He atom impact, but only with collision energy below 600 eV [44]; De Heer and Van Den Bos measured the excitation cross sections for He^{1+} incident on He, but only for excitations to states with principle quantum number $n \geq 3$ [45]. Instead of fitting the data to obtain the excitation cross sections, we estimate the excitation yield $Y_{ex} = N_{ex}/E$ based on the known electronic stopping power as follows. The electronic stopping power $S_e(E)$ can be written as

$$\frac{S_e}{N} = F^\infty_0[\sigma^0_{ion}(Q_{He} + \bar{\varepsilon}_0) + \sigma^0_{ex}\bar{Q}_{ex} + (\sigma^{01} + 2\sigma^{02})(Q_{He} + \lambda E)] + F^\infty_1[\sigma^{1+}_{ion}(Q_{He} + \bar{\varepsilon}_1) + \sigma^{1+}_{ex}\bar{Q}_{ex} + \sigma^{12}(Q_{He} + \lambda E)] + F^\infty_2[\sigma^{2+}_{ion}(Q_{He} + \bar{\varepsilon}_2) + \sigma^{2+}_{ex}\bar{Q}_{ex}]. \quad (8)$$

Here $Q_{He} = 24.6$ eV is the ionization energy of a helium atom. $\bar{\varepsilon}$ is the average kinetic energy of secondary electrons by He ion impact. $\bar{Q}_{ex} = \sum Q_{ij}\sigma_{ij}/\sum \sigma_{ij}$ is the mean excitation energy where Q_{ij} and σ_{ij} are the He$(i \rightarrow j)$ excitation energy and the associated cross section, respectively. Since that the dominant excitation process in low energy collisions between He atoms and the projectile is He$(1s^2 \rightarrow 1s2p)$ with an excitation energy of 21.2 eV [44], and that the cross section decreases drastically with increasing transition energy, we take $\bar{Q}_{ex} \simeq 21$ eV for the incident He ion in all charge states. $\lambda = m_e/m_{He} \simeq 1.36 \times 10^{-4}$ where m_e and m_{He} are the masses of an electron and a He atom, respectively. In Eq. (8), the energy transfer model is assumed such that in a charge-loss collision, a stripped electron is ejected from the projectile with nearly the same velocity as the projectile. Indeed the stripped electrons are observed in the spectrum of secondary electrons produced when He ion impacts on water

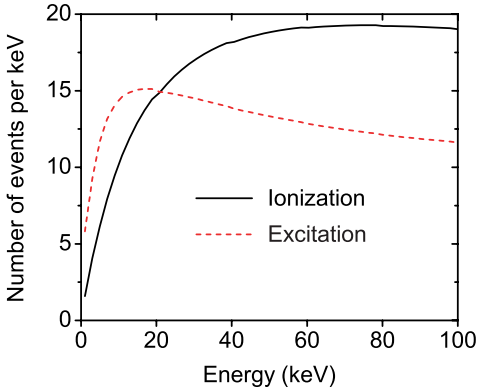

FIG. 6 (color online). Ionization and excitation yields of a recoil He ion in liquid helium as a function of the He ion energy.

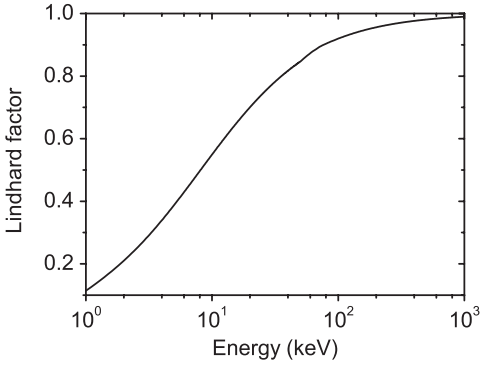

FIG. 7. Calculated Lindhard factor for a recoil He ion in liquid helium as a function of the He ion energy.

vapor as a peak centered at λE [46]. An energy deposition of $Q_{\rm He} + \lambda E$ is thus made when an electron is lost from the projectile [47]. In an electron capture process, energy deposition is essentially due to the recoil of the ionized He atom and is negligible. As a result, the terms in the square brackets in Eq. (7) can be derived based on Eq. (8)

$$\begin{aligned} &F_0^\infty \sigma_{\rm ex}^0 + F_1^\infty \sigma_{\rm ex}^{1+} + F_2^\infty \sigma_{\rm ex}^{2+} \\ &\quad = \frac{1}{\bar{Q}_{\rm ex}} \Big\{ \frac{S_e}{N} - F_0^\infty [\sigma_{\rm ion}^0 (Q_{\rm He} + \bar{\varepsilon}_0) \\ &\qquad + (\sigma^{01} + 2\sigma^{02})(Q_{\rm He} + \lambda E)] \\ &\qquad - F_1^\infty [\sigma_{\rm ion}^{1+} (Q_{\rm He} + \bar{\varepsilon}_1) + \sigma^{12} (Q_{\rm He} + \lambda E)] \\ &\qquad - F_2^\infty [\sigma_{\rm ion}^{2+} (Q_{\rm He} + \bar{\varepsilon}_2)] \Big\}. \end{aligned} \tag{9}$$

Plugging Eq. (9) back into Eq. (7), the excitation yield can be derived as

$$\begin{aligned} Y_{\rm ex} \simeq{}& \frac{L}{\bar{Q}_{\rm ex}} - \frac{Q_{\rm He}}{\bar{Q}_{\rm ex}} Y_{\rm el} - \frac{1}{E} \int_0^E \frac{N dE'}{S(E')} \frac{1}{\bar{Q}_{\rm ex}} \cdot \{ [F_0^\infty \sigma_{\rm ion}^0 \bar{\varepsilon}_0 \\ &+ F_1^\infty \sigma_{\rm ion}^{1+} \bar{\varepsilon}_1 + F_2^\infty \sigma_{\rm ion}^{2+} \bar{\varepsilon}_2] + [F_0^\infty (\sigma^{01} + 2\sigma^{02}) \lambda E \\ &+ F_1^\infty \sigma^{12} \lambda E] \} \end{aligned} \tag{10}$$

in which L is the Lindhard factor, defined as

$$L = \frac{1}{E} \int_0^E \frac{S_e(E') dE'}{S(E')}. \tag{11}$$

The Lindhard factor designates the ratio of the energy given to the electronic collisions to the total energy. A plot of the Lindhard factor as a function of the recoil He ion energy is shown in Fig. 7. Since only the part of energy given to the electronic collisions can be used as ionization and scintillation signals, the Lindhard factor L is important for the determination of the sensitivity of WIMP detectors.

In order to calculate $Y_{\rm ex}$ using Eq. (10), we need to make further approximation on $\bar{\varepsilon}$. The average energy $\bar{\varepsilon}$ of the secondary electrons can be expanded in power series of E. To the lowest order in E, we may write $\bar{\varepsilon} \simeq \gamma(E - 24.6\ {\rm eV})$ for $E > 24.6$ eV. Linear dependence of $\bar{\varepsilon}$ on E is evidenced for secondary electrons ejected by helium ion impact on water vapor with energy $E \lesssim 100$ keV [47]. Furthermore, at small E, $\bar{\varepsilon}$ is similar for He ion impact in different charge states. We choose $\gamma = 0.3$ for all charge states such that the ratio between the calculated ionization yield $Y_{\rm el}$ and excitation yield $Y_{\rm ex}$ agrees with Sato *et al.*'s result at $E \sim 100$ keV where the Lindhard effect is mild. Note that variation of γ does not affect $Y_{\rm ex}$ at small E. The calculated $Y_{\rm ex}$ is shown in Fig. 6 as the red dashed curve.

The drop of both the ionization yield and the excitation yield at energies lower than about 50 keV is due to the drop of the electronic collision cross sections in this energy regime, as well as the loss of the He ion energy to elastic nuclear collisions (Lindhard effect). As a comparison, for an energetic electron moving in LHe, Sato *et al.* [42,48] estimated that the total ionization yield and excitation yield are nearly constant ($Y_{\rm el}^{(e)} \simeq 22.7\ {\rm keV}^{-1}$ and $Y_{\rm ex}^{(e)} \simeq 10.2\ {\rm keV}^{-1}$) in the energy range from a few hundred keV down to about 1 keV.

B. Detectable signals from different channels

1. Charge signal

Electrons and helium ions are produced along the track of an energetic particle as a consequence of ionization or charge-exchange collisions. Beside these processes, excited helium atoms produced by the projectile with principal quantum number $n \geq 3$ can autoionize in liquid helium by the Hornbeck-Molnar process [49],

$$\mathrm{He}^* + \mathrm{He} \rightarrow \mathrm{He}_2^+ + e^-, \tag{12}$$

since the 2 eV binding energy of He^{+2} is greater than the energy to ionize a He($n \geq 3$) atom. Based on the oscillator strengths for the transitions between the ground state and the various excited states of helium [50], slightly more than one third of the atoms promoted to excited states will have a principal quantum number of 3 or greater. All these electrons

and ions quickly thermalize with the liquid helium. The ions form helium "snowballs" in a few picoseconds [51], and they do not move appreciably from the sites where they are originated. On the other hand, as the energy of the free electrons drops below about 20 eV, the only process by which they can lose energy is elastic scattering from helium atoms. Due to the low energy-transfer efficiency (about $\lambda = 1.36 \times 10^{-4}$ per collision), these electrons make many collisions and undergo a random walk until their energy drops below 0.1 eV, the energy thought to be necessary for bubble state formation. Once thermalized, the electrons form bubbles in the liquid typically within 4 ps [52]. Due to the Coulomb attraction, electron bubbles and helium ion snowballs recombine in a very short time and lead to the production of He_2^* excimer molecules:

$$(He_3^+)_{\text{snowball}} + (e^-)_{\text{bubble}} \rightarrow He_2^* + He. \qquad (13)$$

When an external electric field is applied, some of the electrons can escape the recombination and be extracted.

At temperatures above 1 K, electron bubbles essentially move along the electric field lines in the moving frame of the ions due to the viscous damping [53,54]. In this situation, the fraction q of the electrons that can be extracted under an applied field ε depends largely on the initial electron-ion separation and the ionization density along the projectile track. The mean electron-ion separation has been determined to be about 60 nm for both beta particle ionization events [54] and alpha particle ionization events [55]. The energy deposition rate for an electron of several hundred keV is approximately 50 eV/micron, whereas for an alpha particle of a few MeV the rate is 25 keV/micron [56]. The average energy needed to produce an electron-ion pair has been measured to be about 42.3 eV for a beta particle [57] and about 43.3 eV [58] for an alpha particle. It follows that charge pairs are separated on average about 850 nm along a beta particle track and only about 1.7 nm along the track of an energetic alpha particle. The recombination along a beta particle track where the electron-ion pairs are spatially separated is described by Onsager's geminate recombination theory [59]. For the highly ionizing track of an alpha particle in liquid helium, the electrons feel the attraction from all nearby ions and are harder to be extracted. Jaffe's columnar theory of recombination is more applicable in this situation [60,61]. In Fig. 8, the charge extraction from a beta particle track, simulated by Guo *et al.* [54], and that from an alpha particle track, simulated by Ito *et al.* [55], are shown as the blue solid curve and the red dashed curve, respectively. Note that in the low field regime, the measured charge collection by Ghosh [62] and Sethumadhavan [63] for beta particles is higher than the predicted result by Guo *et al.* [54]. Furthermore, these charge extraction analyses are for temperatures above 1 K. At very low temperatures, the ionized electrons can stray away from the field lines which enhances the charge extraction at a given applied field [54].

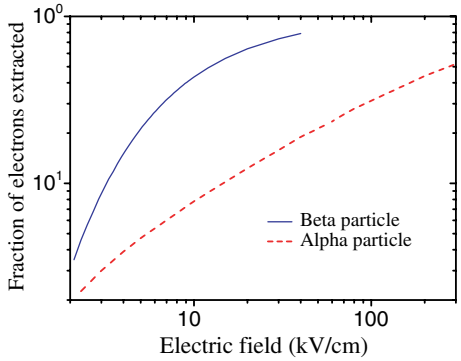

FIG. 8 (color online). Electron extraction fraction q as a function of the drift electric field. The blue solid curve represents the simulated electron extraction from beta tracks by Guo *et al.* [54]. The red dashed curve represents the simulated electron extraction from alpha tracks by Ito *et al.* [55]. Note that fields up to 40 kV/cm have been readily applied in liquid helium [55].

The mean electron-ion separation along the track of a low energy recoil He nuclei should be similar to that for beta and alpha particles. The ionization density along the He nuclei track can be estimated by $(N_{\text{el}} + \frac{1}{3}N_{\text{ex}})/Z$, where $Z = \int_0^E dE'/S(E')$ is the track length of the recoil He ion. Due to the Lindhard effect, a major part of the projectile energy is lost to elastic collisions at small E. Consequently, the ionization density along the track of a recoil He ion should be much lower than that along the track of an energetic alpha particle. For instance, for a 10 keV recoil He nuclei, the ions produced are on average separated by about 20 nm along the track. At lower recoil energies, the separation between ionizations becomes comparable or even larger than the mean electron-ion separation. As a consequence, the charge extraction fraction q for low energy nuclear recoils is expected to be similar to that for electron recoils. Due to the lack of experimental information, in the following analysis we assume the same q for both low energy recoil He nucleus and beta particles. The charge counts S2 for nuclear recoils and electron recoils are thus given by $q(Y_{\text{el}} + \frac{1}{3}Y_{\text{ex}})E$ and $q(Y_{\text{el}}^{(e)} + \frac{1}{3}Y_{\text{ex}}^{(e)})E$, respectively. Note that the terms $\frac{1}{3}Y_{\text{ex}}$ and $\frac{1}{3}Y_{\text{ex}}^{(e)}$ account for the ionizations produced by the autoionization of the excited He atoms.

2. Excitations and scintillation

Excited helium atoms can be produced in excitation collisions. For electron recoils, Sato *et al.* [48] calculated that 83% of the excited helium atoms produced in excitation collisions are in the spin-singlet states and the remaining 17% are in triplet states. For low energy nuclear recoils, however, the direct excitations are nearly all to spin-singlet states [42,44]. This is because that since the total spin is conserved, excitation to triplet states can occur only when both the recoil He and the ground state He atom are excited

simultaneously to triplet states. This process requires more energy and has a lower chance to occur. The excited atoms are then quickly quenched to their lowest energy singlet and triplet states, $He^*(2^1S)$ and $He^*(2^3S)$, and react with the ground state helium atoms of the liquid, forming excited $He_2(A^1\Sigma_u)$ and $He_2(a^3\Sigma_u)$ molecules:

$$He^* + He \rightarrow He_2^*. \tag{14}$$

He_2^* excimer molecules are also produced as a consequence of recombinations of electron-ion pairs. For geminate recombination, experiments [56] indicate that roughly 50% of the excimers that form on recombination are in excited spin-singlet states and 50% are in spin-triplet states. He_2^* molecules in highly excited singlet states can rapidly cascade to the first-excited state, $He_2(A^1\Sigma_u)$, and from there radiatively decay in less than 10 ns to the ground state [64], $He_2(X^1\Sigma_g)$, emitting ultraviolet photons in a band from 13 to 20 eV and centered at 16 eV. As a consequence, an intense prompt pulse of extreme-ultraviolet scintillation light is released following an ionizing radiation event. These photons can pass through bulk helium and be detected since there is no absorption in helium below 20.6 eV.

The radiative decay of the triplet molecules $He_2(a^3\Sigma_u)$ to the singlet ground state $He_2(X^1\Sigma_g)$ is forbidden since the transition involves a spin flip. The radiative lifetime of an isolated triplet molecule $He_2(a^3\Sigma_u)$ has been measured in liquid helium to be around 13 s [65]. The triplet molecules, resulting from both electron-ion recombination and from reaction of excited triplet atoms, diffuse out of the ionization track. They may radiatively decay, react with each other via bimolecular Penning ionization [66], or be quenched at the container walls. Experimentally, these molecules can be driven by a heat current to quench on a metal detector surface and be detected as a charge signal [67,68].

Note that nonradiative destruction of singlet excimers by the bimolecular Penning ionization process can lead to the quenching of the prompt scintillation light. Such quenching effect has been observed for energetic alpha particles in liquid helium [56,69]. At temperatures above 2 K, the singlet excimers can diffuse on the order of 10 nm in their 10 ns lifetime [70]. Based on the discussion presented in the previous section, the mean separation of the excimers along the track of a low energy recoil helium can be greater than the diffusion range of the singlet excimers. The quenching of the prompt scintillation for low energy nuclear recoils should thus be small. At low temperatures, the quenching effect may be significant. However, it has been observed that even for the highly ionizing track of an energetic alpha particle, the light quenching becomes mild below about 0.6 K [69]. This is presumably due to the trapping of the excimers on quantized vortex lines that are created accompanying the energy deposition of the recoil helium [68]. Such trapping limits the motion of the excimers and hence reduces the light quenching. A reliably estimation of the quenching effect is not feasible due to the lack of experimental knowledge about the decay rates at which bimolecular Penning processes occur among the different excimers. Considering the fact that the quenching effect could be small, we shall not include the quenching analysis in our model.

For convenience, in the following discussion, we will use the same notations as being commonly used in the xenon detector community: S1 representing the counts of the prompt scintillation photons, and S2 representing the counts of the extracted charges. We also consider the signal from the long-lived triplet helium molecules, which will be denoted as S3.

Based on the above discussion, the prompt scintillation photons ($S1^{(e)}$) and triplet molecules ($S3^{(e)}$) produced by an electron recoil event are given by

$$S1^{(e)} = E \cdot \left[Y_{\rm el}^{(e)} \cdot (1-q) \cdot 50\% + Y_{\rm ex}^{(e)} \cdot 86\% \cdot \frac{2}{3} + Y_{\rm ex}^{(e)} \cdot 86\% \cdot \frac{1}{3} \cdot (1-q) \right], \tag{15}$$

$$S3^{(e)} = E \cdot \left[Y_{\rm el}^{(e)} \cdot (1-q) \cdot 50\% + Y_{\rm ex}^{(e)} \cdot 14\% \cdot \frac{2}{3} + Y_{\rm ex}^{(e)} \cdot 14\% \cdot (1-q) \cdot \frac{1}{3} \right]. \tag{16}$$

The factor $2/3$ accounts for the fraction of the excited atoms that do not undergo autoionization. The above two formulas assume that the recombination of electron-ion pairs produced by the autoionization of singlet (or triplet) helium atoms tends to generate only singlet (or triplet) helium excimers. The justification for this assumption is that the energy of the electrons produced in the Hornbeck-Molnar process is low (less than 2 eV). These electrons do not move very far from their parent ions, hence their spin correlation with their parent ions is likely strong enough to survive the whole ionization-recombination process. As for the nuclear recoils, the $S1^{(n)}$ and $S3^{(n)}$ counts are given by

$$S1^{(n)} = E \cdot \left[Y_{\rm el} \cdot (1-q) \cdot 50\% + Y_{\rm ex} \cdot \frac{2}{3} + Y_{\rm ex} \cdot \frac{1}{3} \cdot (1-q) \right], \tag{17}$$

$$S3^{(n)} = E \cdot Y_{\rm el} \cdot (1-q) \cdot 50\%. \tag{18}$$

Since the excited atoms are assumed to be all in singlet states for nuclear recoils, the triplet molecules are generated solely as a consequence of the recombination of charge pairs produced in direct ionization collisions.

For the readers' convenience, in Table I, we summarize the formulas that we used to estimate the S1, S2, and S3 counts for both nuclear recoils and electron recoils with incident energy of E.

TABLE I. The yields of prompt scintillation (S1), charge (S2), and He_2^* triplet molecules (S3) for nuclear recoils and electron recoils with incident energy of E in liquid helium.

	Nuclear recoils	Electron recoils
S1	$E \cdot [0.5 \cdot Y_{el} \cdot (1-q) + 0.67 \cdot Y_{ex} + 0.33 \cdot Y_{ex} \cdot (1-q)]$	$E \cdot [0.5 \cdot Y_{el}^{(e)} \cdot (1-q) + 0.57 \cdot Y_{ex}^{(e)} + 0.29 \cdot Y_{ex}^{(e)} \cdot (1-q)]$
S2	$E \cdot (Y_{el} + 0.33 \cdot Y_{ex}) \cdot q$	$E \cdot (Y_{el}^{(e)} + 0.33 \cdot Y_{ex}^{(e)}) \cdot q$
S3	$E \cdot Y_{el} \cdot 0.5 \cdot (1-q)$	$E \cdot [0.5 \cdot Y_{el}^{(e)} \cdot (1-q) + 0.093 \cdot Y_{ex}^{(e)} + 0.047 \cdot Y_{ex}^{(e)} \cdot (1-q)]$

III. DISCRIMINATION OF NUCLEAR RECOILS AND ELECTRON RECOILS

The success of a dark-matter direct detection experiment will depend in its ability to distinguish between electron recoils and nuclear recoils. In this section, we present results of Monte Carlo simulations showing that excellent background rejection can be achieved for the purpose of WIMP dark matter detection, based on the ratios of the counts from different signals.

A. Ratios of the signals from different channels

Discrimination between both types of recoils can be done by looking at the ratio of the counts from different signal channels. These ratios depend on the event type, the recoil energy, and the applied electric field. The formulas listed in Table I allow us to estimate these ratios. As an example, in Fig. 9, the calculated ratios of S2/S1 and S3/S1 are shown as a function of the electric field for both the electron recoils and nuclear recoils with a recoil energy of 10 keV. The S2/S1 ratio for both electron recoils and nuclear recoils increases with the applied electric field. This is because at higher fields more electrons can be extracted, which enhances the S2 counts and in the meanwhile reduces the S1 counts since less electrons recombine with the ions to form singlet molecules. The difference of the S2/S1 ratio between electron recoils and nuclear recoils becomes greater at higher fields, which means that better discrimination based on S2/S1 can be achieved at higher fields.

In Fig. 10, we show the calculated ratios of S2/S1 and S3/S1 as a function of the event energy for both electron recoils and nuclear recoils at an assumed field of 10 kV/cm. Since we take the ionization and excitation yields for electron recoils to be constants, the S2/S1 and S3/S1 ratios for electron recoils are independent of the recoil energy. For nuclear recoils, both the S2/S1 and S3/S2 ratios decrease with decreasing recoil energy. Note that the ratios evaluated here are based on the calculated average counts from the different signal channels. In real experiment, there always exist number uncertainties of the counts. At low recoil energies where the counts are small, the relative uncertainties of the counts as well as the ratios of the counts between different channels become large, which limits the discrimination of the two types of recoils. For the helium detector, as we can see from Fig. 10, the S2/S1 and S3/S1 curves for nuclear recoils bend away from those for electron recoils, which compensates the effect due to count uncertainty. As we shall show later, excellent event discrimination can still be achieved even down to a few keV energy regime.

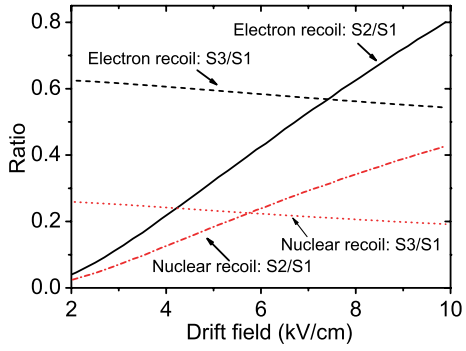

FIG. 9 (color online). The ratio of the counts from different signal channels for 10 keV nuclear recoil and electronic recoil events as a function of the electric field.

B. Relative scintillation efficiency

The quantities that can be measured experimentally for a recoil event are the counts from the different signal channels. One can plot, for instance, the S2/S1 ratio against the S1 counts. However, the conversion between S1 counts to the event energy is different for electron recoils and nuclear recoils. For electron recoils, the event energy is proportional to the mean S1 counts, since the ionization and the excitation yields are taken to be constant. For nuclear recoils, such conversion is nonlinear. The relative

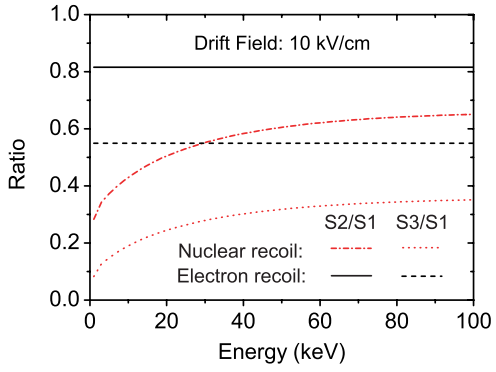

FIG. 10 (color online). The ratio of the counts between different signal channels for nuclear recoil and electron recoil events as a function of the event energy. The electric field strength assumed in the simulation is 10 kV/cm.

scintillation efficiency $L_{\rm eff}$ describes the difference between the amount of energy measured in the detector between both types of recoils. In the notation used in the field, the keV electron equivalent scale (keVee) is used to quantify a measured signal in terms of the energy of an electron recoil that would be required to generate it. Similarly the keVnr scale is used for nuclear recoil events. For an electron recoil of energy E_e, the nuclear recoil event that would produce an equivalent mean S1 signal is given by $E_{nr} = E_e \cdot (S_e/S_n)L_{\rm eff}^{-1}$. S_e and S_n denote the light quenching factors due to an applied electric field for electron recoils and nuclear recoils, respectively.

Experimentally, the conversion between S1 and the electron equivalent scale keVee can be established using gamma line sources, for example the ^{57}Co 122 keV line. The nuclear recoil response as a function of energy can be established using neutron scattering. Using the formulas listed in Table I, we can determine the $L_{\rm eff}$ by calculating the ratio of the energies of the two types of recoil events that give the same mean S1 counts under zero electric field. The result is shown in Fig. 11(a). For completeness, the calculated S_n as a function of event energy at a few fields are shown in Fig. 11(b). Note that in our model, S_e does not depend on event energy. We determine that $S_e = 0.69$, 0.55, and 0.44 for fields at 10 kV/cm, 20 kV/cm, and 40 kV/cm, respectively.

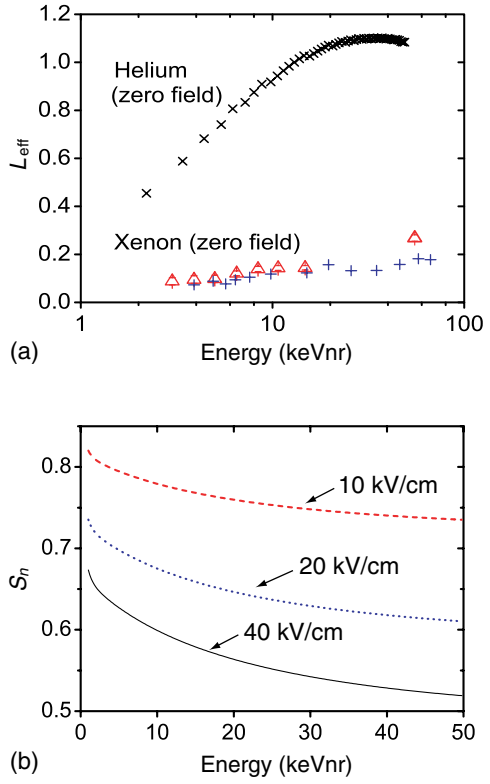

FIG. 11 (color online). (a) The relative scintillation efficiency $L_{\rm eff}$ as a function of the recoil event energy. The × represents the calculated $L_{\rm eff}$ for helium under zero electric field. The measured data for liquid xenon by Plante *et al.* [71] [red (light gray) open triangle] and by Manzur *et al.* [38] (positive sign) are also shown. (b) The calculated light quenching factor S_n for nuclear recoils as a function of event energy, for fields at 10 kV/cm, 20 kV/cm, and 40 kV/cm, respectively.

The event discrimination ability of a detector drops drastically below a certain threshold S1 counts. For a given energy threshold in keVee scale, a detector with a higher $L_{\rm eff}$ has lower nuclear recoil energy threshold, hence would be sensitive to low energy WIMPs. In Fig. 11(a), we also show the experimentally measured $L_{\rm eff}$ data for liquid xenon [38,71]. In the low energy regime of a few keV, the xenon-based detector only has a $L_{\rm eff}$ of less than 0.1 while the helium detector has a $L_{\rm eff}$ above 0.4. So while liquid helium has substantially lower scintillation yield for electron recoils, this is unlikely to be the case for nuclear recoils.

C. Rejection power

The uncertainty of the signal counts limits the discrimination between the nuclear recoils and the electron recoils at low energies. To study this effect, we performed a Monte Carlo simulation similar to the analysis that has been done for xenon-based detectors [72]. The energy E_e of the event in electron equivalent units is sampled. The corresponding nuclear recoil energy E_r is found based on the conversion discussed in the previous section. The mean counts of the ionizations and the excitations for a nuclear recoil with energy E_r and for an electron recoil with energy E_e are calculated using the formulas listed in Table I. We then introduce the count fluctuations in each of the steps that lead to the final detectable signals. A detailed description on generating the signal fluctuations for a nuclear recoil event is given below. The analysis for an electron recoil is similar.

We first generate the ionization counts $N_{\rm ion}^{(n)}$ and the excitation counts $N_{\rm ex}^{(n)}$ for the nuclear recoil event based on Poisson distributions around their mean values in each trial of the Monte Carlo simulation. The total ionization counts $N_{\rm ion,sum}$ is the sum of the direct ionizations and the autoionizations, where the autoionization counts are generated based on a binomial distribution with 1/3 success probability and with total trials of $N_{\rm ex}^{(n)}$. The extracted-charge counts (S2) are then generated based on a binomial distribution with $N_{\rm ion,sum}$ total trials and with a success probability of the yield factor q under a given electric field. Here we assume that the extracted charges can all be detected by means of standard charge amplification methods such as the proportional scintillation in a two-phase chamber that has been used in argon, krypton, and xenon detectors [73–76], or the electron avalanche in a gas electron multiplier (GEM) [77–79]. The rest ion-electron pairs recombine and generate singlet molecules based on a binomial distribution with 50% success probability. The total singlet molecules are the sum of the counts from the

ion-electron recombination and from the singlet excitations. The prompt scintillation counts (S1) are finally generated based on a binomial distribution with total trials of the total number of singlet molecules, and with a success probability of the detection efficiency (e.g., 20% typical for a two-phase detector).

The ratios of S2/S1 for a nuclear recoil and for an electron recoil are evaluated and represented by a red dot and a black dot in the S2/S1 versus S1 plot. 10^7 trials are carried out for a given electric field strength and the S1 collection efficiency. An example is shown in Fig. 12(a). A clear separation can be seen between the electron recoil band and the nuclear recoil band, a necessary criterion for any direct dark matter experiment. At low energies where the S1 counts are small, the two bands overlap due to the relatively large scattering of the S2/S1 value. The solid curve shown in Fig. 12(a) is the calculated mean S2/S1 as a function of the mean S1 counts for nuclear recoils. The mean counts are directly related to the event energy. For example, for a nuclear recoil with energy $E_r = 5$ keV under an electric field of 10 kV/cm, on average about 59 prompt scintillation photons will be generated, leading to a mean S1 signal of about 12 counts, assuming 20% photon-collection efficiency. We also expect that about 22 electrons (S2) will be collected. Considering count fluctuations, monoenergetic events will have a distribution on the S2/S1 versus S1 plot. In Fig. 12(b), we show the distributions of monoenergetic nuclear recoils and electron recoils at 10 keVee, 25 keVee, and 40 keVee. The shapes of these distributions are similar to those for xenon detectors that are derived by Sorensen [80].

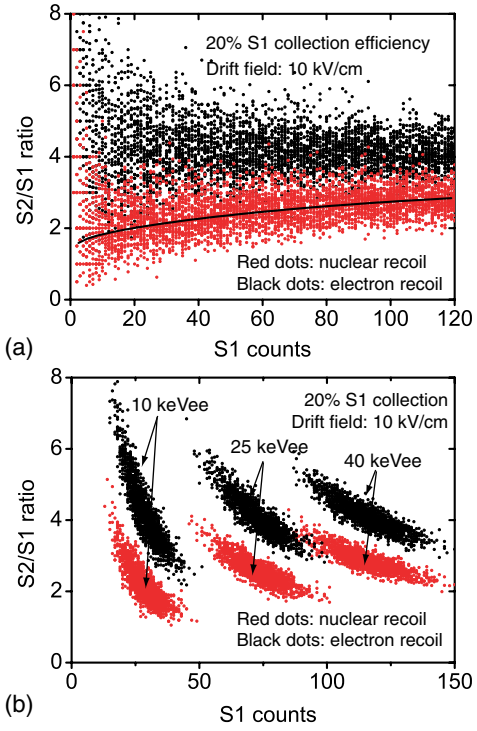

FIG. 12 (color online). (a) Monte Carlo simulation of the S1/S2 ratio for nuclear recoils (red dots) and electron recoils (black dots). The S1 scintillation light collection efficiency is assumed to be 20%. The electric field strength assumed in the simulation is 10 kV/cm. The black solid curve shows the calculated mean S2/S1 as a function of S1 counts for nuclear recoils. (b) Distribution of monoenergetic nuclear recoils and electron recoils on the S2/S1 versus S1 plot.

To calculate the efficiency of rejecting electron recoils for a given electron recoil energy E_e (the rejection power), we first generate monoenergetic electron recoils on the S2/S1 versus S1 plot, like those shown in Fig. 12(b). The rejection power is then calculated as the fraction of the electron recoils that appear below the nuclear recoil band centroid, e.g., the solid curve shown in Fig. 12(a). A full description on calculating the rejection power can be found in the literature [72,81].

We considered fields up to 40 kV/cm in the calculation. It has been shown that such high fields can be readily applied in liquid helium [55]. Indeed, the design electric field value of the Spallation Neutron Source (SNS) neutron EDM experiment is 50 kV/cm [82–84]. The calculated rejection power curves as a function of event energy in keVee scale at several electric fields and with different S1 collection efficiencies are shown in Fig. 13. At low energies, the ability to distinguish electron and nuclear recoils is degraded because of the lack of charge and light signal. But above a few keV, rejection power is predicted to improve considerably, and this should allow for low-background operation and a sensitive WIMP search. The discrimination is better at higher fields or with higher S1 collection efficiency. For a single-phase helium detector operated at very low temperatures, sensitive bolometers immersed in liquid helium may be used to read out the light and the charge signals. In this case, 80% S1 collection may be possible with the detector inner surface being covered by bolometer arrays. Note that the rejection power analysis is based on the charge extraction curve shown in Fig. 8. The actual charge extraction at a given field could be higher, such as measured by Ghosh [62] and Sethumadhavan [63].

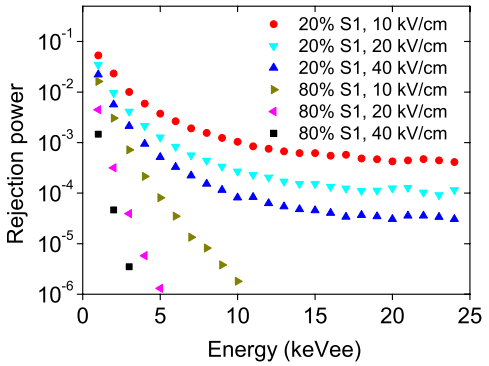

FIG. 13 (color online). Calculated rejection power for a helium detector as a function of event energy in keVnr scale.

At low temperatures the ionized electrons can stray away from field lines, which may also lead to higher charge extraction [54]. This will result in even more efficient electron recoil versus nuclear recoil discrimination.

It is worthwhile mentioning that at low temperatures, metastable helium molecules in triplet state can drift at a speed of a few meters per second [68]. When these molecules collide on the bolometer surface, they undergo nonradiative quenching and release over 10 eV of energy depending on the material of the impinged surface. A significant amount of this energy will be deposited into the calorimetric sensor, which may allow us to detect the triplet molecule signal (S3). A combined analysis of S2/S1 and S3/S1 ratios may further improve the rejection power of the detector.

IV. SENSITIVITY

For dark matter detection, we have considered various schemes for implementing the detector, including temperature and readout. We propose to detect both prompt scintillation and charge in liquid helium-4, using a time projection chamber design. This is essentially the same approach used in Ar and Xe detectors [73–75], which has proven to be very effective, providing excellent position resolution and electron recoil discrimination. The detector may be operated either at high temperature regime ($\sim$3 K) using photomultiplier tube arrays for signal readout, or at low temperatures ($\sim$100 mK) using bolometer arrays for signal readout. A discussion of the proposed helium detectors will be published in the future.

As explained in Sec. I, a useful figure of merit for light WIMP searches is (nuclear mass) $\times$ (energy threshold), which must be minimized to get the best light WIMP sensitivity. In the case of liquid helium, this must be balanced with the background reduction achieved through discrimination of electron recoil events, which improves with higher energy. Given helium's large predicted nuclear recoil signals and excellent discrimination, we expect an energy threshold of about 4–5 keV with photomultiplier readout, potentially reducible to 1–3 keV with bolometric readout. The low nuclear mass of helium then gives access to very low WIMP masses, while still having significant background reduction through discrimination.

While liquid helium will not provide significant self-shielding against gamma rays (a significant background rejection method in LXe and LAr detectors), a plausible background rate of 10^{-3} events/day/keVee/kg after discrimination will allow excellent sensitivity to light WIMPs, for which current experimental sensitivities are relatively weak. A detailed discussion of the background of a helium detector designed for the HERON project was given by Huang *et al.* [85]. For a 0.5 kg helium fiducial mass, 20% light collection, a 20 kV/cm drift field, an energy threshold of 4.8 keV, 300 days of operation, and a 95% efficient gamma ray veto, one background event is predicted, with a WIMP-nucleon cross-section sensitivity of 2×10^{-42} cm^2 at 9 GeV. This cross-section sensitivity is an order of magnitude lower than the highest likelihood cross section from the silicon detectors of the CDMS-II experiment, when interpreted under a WIMP plus background hypothesis [86]. Sensitivity may be improved further with higher drift fields, more efficient light collection, and larger exposure, potentially reaching 10^{-44} cm^2 or better between 2–20 GeV. Some predicted light WIMP sensitivities are summarized above in Fig. 14.

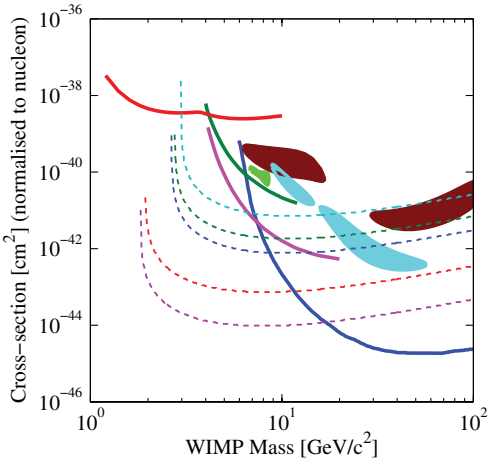

FIG. 14 (color online). Spin-independent WIMP exclusion curves (solid lines), potential WIMP signals (solid regions), and projected liquid helium 90% sensitivity curves (dashed lines) in the region of 1–100 GeV WIMP mass. Exclusion curves include DAMIC in red [108], CDMS-II in green [10], XENON10 in magenta [12], and XENON100 in blue [14]. Potential WIMP signals include DAMA in red [109], CRESST in light blue [17], and CoGeNT in green [16]. Projected liquid helium sensitivities for different detector parameters are shown as dashed lines, including light blue (10 kV/cm, 20% S1 collection, 4.8 keV threshold), green (20 kV/cm, 20% S1 collection, 4.4 keV threshold), blue (40 kV/cm, 20% S1 collection, 4.2 keV threshold), red (20 kV/cm, 80% S1 collection, 2.8 keV threshold), and magenta (40 kV/cm, 80% S1 collection, 2.6 keV threshold). Predicted limits assume an electron recoil background of 1 event/keVee/kg/day and a 95% efficient gamma ray veto. Existing exclusion curves and potential WIMP signal regions are generated using DMTools [110].

V. CONCLUSION

We conclude that liquid helium is an intriguing material for the direct detection of light WIMPs, as it combines multiple signal channels, comparatively large signals for nuclear recoils, a low target mass, and the capacity for electron recoil discrimination. As revealed in our analysis, a high electric field is needed to extract electrons from nuclear recoil tracks, allowing a sizable charge signal for time projection chamber readout, and good position resolution. Before dark matter experiments can be performed with this technology, a method of detecting single electrons in liquid superfluid helium must be demonstrated.

In addition, detailed measurements must be done of the nuclear and electron recoil signal and discrimination efficiency at low energies.

ACKNOWLEDGMENTS

We thank R. E. Lanou, D. Hooper, D. Prober, T. M. Ito, G. M. Seidel, H. J. Maris, and A. Buzulutskov for valuable discussions and comments, and D. Klemme for her assistance in preparation of this manuscript. We also acknowledge useful comments by the anonymous reviewer. W. G. is supported by the startup grant provided by Florida State University and the National High Magnetic Field Laboratory. D. N. M. is supported by the National Science Foundation, Grant No. PHY-1003660.

[1] D. N. Schramm, Proc. Natl. Acad. Sci. U.S.A. **95**, 42 (1998).
[2] W. Hu, Astrophys. J. Lett. **557**, L79 (2001).
[3] M. Tegmark *et al.* (SDSS Collaboration), Astrophys. J. **606**, 702 (2004).
[4] Y. Mellier, Annu. Rev. Astron. Astrophys. **37**, 127 (1999).
[5] M. W. Goodman and E. Witten, Phys. Rev. D **31**, 3059 (1985).
[6] G. Jungman, M. Kamionkowski, and K. Griest, Phys. Rep. **267**, 195 (1996).
[7] J. Giedt, A. W. Thomas, and R. D. Young, Phys. Rev. Lett. **103**, 201802 (2009).
[8] H. Goldberg, Phys. Rev. Lett. **50**, 1419 (1983).
[9] J. R. Ellis, J. S. Hagelin, D. V. Nanopoulos, K. A. Olive, and M. Srednicki, Nucl. Phys. **B238**, 453 (1984).
[10] Z. Ahmed *et al.* (CDMS-lite Collaboration), Phys. Rev. Lett. **106**, 131302 (2011); Z. Ahmed *et al.*, Phys. Rev. Lett. **102**, 011301 (2009).
[11] D. Akimov *et al.*, Phys. Lett. B **709**, 14 (2012).
[12] J. Angle *et al.* (XENON10 Collaboration), Phys. Rev. Lett. **107**, 051301 (2011).
[13] E. Aprile *et al.*, Phys. Rev. Lett. **105**, 131302 (2010).
[14] E. Aprile *et al.* (XENON100 Collaboration), Phys. Rev. Lett. **109**, 181301 (2012).
[15] R. Bernabei *et al.*, Eur. Phys. J. C **67**, 39 (2010).
[16] C. E. Aalseth *et al.* (COGENT Collaboration), Phys. Rev. Lett. **106**, 131301 (2011); C. E. Aalseth *et al.*, Phys. Rev. Lett. **107**, 141301 (2011).
[17] G. Angloher *et al.*, Eur. Phys. J. C **72**, 1971 (2012).
[18] D. Hooper, arXiv:1201.1313.
[19] A. Bottino, N. Fornengo, and S. Scopel, Phys. Rev. D **67**, 063519 (2003); A. Bottino, F. Donato, N. Fornengo, and S. Scopel, Phys. Rev. D **69**, 037302 (2004); J. F. Gunion, D. Hooper, and B. McElrath, Phys. Rev. D **73**, 015011 (2006); A. Bottino, F. Donato, N. Fornengo, and S. Scopel, Phys. Rev. D **78**, 083520 (2008); **77**, 015002 (2008); **81**, 107302 (2010); J. F. Gunion, A. V. Belikov, and D. Hooper, arXiv:1009.2555.
[20] S. Nussinov, Phys. Lett. **165B**, 55 (1985); D. B. Kaplan, Phys. Rev. Lett. **68**, 741 (1992); D. E. Kaplan, M. A. Luty, and K. M. Zurek, Phys. Rev. D **79**, 115016 (2009); J. Shelton and K. Zurek, Phys. Rev. D **82**, 123512 (2010); A. Falkowski, J. T. Ruderman, and T. Volansky, J. High Energy Phys. 05 (2011) 106.
[21] J. L. Feng and J. Kumar, Phys. Rev. Lett. **101**, 231301 (2008); J. Feng, J. Kumar, and L. Strigari, Phys. Lett. B **670**, 37 (2008).
[22] C. P. Burgess, M. Pospelov, and T. ter Veldhuis, Nucl. Phys. **B619**, 709 (2001); S. Andreas, T. Hambye, and M. H. G. Tytgat, J. Cosmol. Astropart. Phys. 10 (2008) 034; Y. G. Kim and S. Shin, J. High Energy Phys. 05 (2009) 036.
[23] B. Holdom, Phys. Lett. **166B**, 196 (1986); D. P. Finkbeiner and N. Weiner, Phys. Rev. D **76**, 083519 (2007); N. Arkani-Hamed and N. Weiner, J. High Energy Phys. 12 (2008) 104; D. Hooper and K. M. Zurek, Phys. Rev. D **77**, 087302 (2008); M. Pospelov, A. Ritz, and M. B. Voloshin, Phys. Lett. B **662**, 53 (2008); K. M. Zurek, Phys. Rev. D **79**, 115002 (2009); N. Arkani-Hamed, D. P. Finkbeiner, T. R. Slatyer, and N. Weiner, Phys. Rev. D **79**, 015014 (2009); C. Cheung, J. T. Ruderman, L.-T. Wang, and I. Yavin, Phys. Rev. D **80**, 035008 (2009); M. Pospelov and A. Ritz, Phys. Lett. B **671**, 391 (2009); R. Essig, J. Kaplan, P. Schuster, and N. Toro, arXiv:1004.0691; D. Hooper, N. Weiner, and W. Xue, Phys. Rev. D **86**, 056009 (2012).
[24] R. Foot, Int. J. Mod. Phys. D **13**, 2161 (2004); Phys. Rev. D **78**, 043529 (2008).
[25] G. Giesen, J. Lesgourgues, B. Audren, and Y. Ali-Haïmoud, J. Cosmol. Astropart. Phys. 12 (2012) 008.
[26] S. Chatrchyan *et al.* (CMS Collaboration), Phys. Rev. Lett. **108**, 261803 (2012); G. Aad *et al.* (ATLAS Collaboration), J. High Energy Phys. 04 (2013) 075.
[27] M. Ackermann *et al.* (Fermi-LAT Collaboration), Phys. Rev. Lett. **107**, 241302 (2011); A. Geringer-Sameth and S. M. Koushiappas, Phys. Rev. Lett. **107**, 241303 (2011).
[28] J. D. Lewin and P. F. Smith, Astropart. Phys. **6**, 87 (1996).
[29] R. E. Lanou, H. J. Maris, and G. M. Seidel, Phys. Rev. Lett. **58**, 2498 (1987); S. R. Bandler, C. Enss, G. Goldhaber, R. E. Lanou, H. J. Maris, T. More, F. S. Porter, and G. M. Seidel, J. Low Temp. Phys. **93**, 785 (1993).
[30] R. E. Lanou, H. J. Maris, and G. M. Seidel, in *Proceedings of the Dark Matter in XXIII Rencontres de Moriond*, edited by J. Adouze and J. Tran Thanh Van (Editions Frontieres, Paris, 1988), pp. 79–83.
[31] J. Adams *et al.*, in *Proceedings of the XXXIst Moriond Conference, Les Arcs, France* (1996), pp. 14–27.
[32] D. I. Bradley, M. R. Follows, W. M. Hayes, and T. Sloan, Nucl. Instrum. Methods Phys. Res., Sect. A **370**, 141 (1996); C. B. Winkelmann, J. Elbs, E. Collin, Y. M. Bunkov, and H. Godfrin, Nucl. Instrum. Methods Phys. Res., Sect. A **559**, 384 (2006); **574**, 264 (2007).
[33] J. M. Doyle and S. K. Lamoreaux, Europhys. Lett. **26**, 253 (1994); P. R. Huffman *et al.*, Nature (London) **403**, 62

(2000); D. N. McKinsey *et al.*, Phys. Rev. A **67**, 062716 (2003); Nucl. Instrum. Methods Phys. Res., Sect. A **516**, 475 (2004).
[34] R. Golub and S. K. Lamoreaux, Phys. Rep. **237**, 1 (1994).
[35] D. H. Beek *et al.*, arXiv:1111.1273.
[36] C. A. Baker *et al.*, J. Phys. Conf. Ser. **251**, 012055 (2010).
[37] J. Lindhard and M. Scharff, Phys. Rev. **124**, 128 (1961).
[38] A. Manzur, A. Curioni, L. Kastens, D. N. McKinsey, K. Ni, and T. Wongjirad, Phys. Rev. C **81**, 025808 (2010).
[39] P. Sorensen and C. E. Dahl, Phys. Rev. D **83**, 063501 (2011).
[40] S. K. Allison, Rev. Mod. Phys. **30**, 1137 (1958).
[41] M. J. Berger, J. S. Coursey, M. A. Zucker, and J. Chang, "Stopping-Power and Range Tables for Electrons, Protons, and Helium Ions," NIST Standard Reference database Number 124, 1998, National Institute of Standards and Technology, Gaithersburg, MD [http://webbook.nist.gov].
[42] S. Sato, K. Kowari, and K. Okazaki, Bull. Chem. Soc. Jpn. **49**, 933 (1976).
[43] L. H. Thomas, Math. Proc. Cambridge Philos. Soc. **23**, 829 (2008).
[44] V. Kempter, V. Veith, and L. Zehnle, J. Phys. B: At. Mol. Phys. **8**, 1041 (1975).
[45] F. J. De Heer and J. Van Den Bos, Physica (Amsterdam) **31**, 365 (1965).
[46] L. H. Toburen, W. E. Wilson, and R. J. Popowich, Radiat. Res. **82**, 27 (1980).
[47] S. Uehara and H. Nikjoo, J. Phys. Chem. B **106**, 11051 (2002).
[48] S. Sato, K. Kowari, and S. Ohno, Bull. Chem. Soc. Jpn. **47**, 2174 (1974).
[49] J. A. Hornbeck and J. P. Molnar, Phys. Rev. **84**, 621 (1951).
[50] J. Berkowitz, J. Phys. B: At., Mol. Opt. Phys. **30**, 881 (1997).
[51] M. Ovchinnikov, B. L. Grigorenko, K. C. Janda, and V. A. Apkarian, J. Chem. Phys. **108**, 9351 (1998).
[52] J. P. Hernandez and M. J. Silver, Phys. Rev. A **2**, 1949 (1970).
[53] W. Guo, D. Jin, G. M. Seidel, and H. J. Maris, Phys. Rev. B **79**, 054515 (2009).
[54] W. Guo, M. Dufault, S. B. Cahn, J. A. Nikkel, Y. Shin, and D. N. McKinsey, JINST **7**, P01002 (2012).
[55] T. M. Ito, S. M. Clayton, J. Ramsey, M. Karcz, C. Y. Liu, J. C. Long, T. G. Reddy, and G. M. Seidel, Phys. Rev. A **85**, 042718 (2012).
[56] J. S. Adams, Ph.D. thesis, Brown University, 2001.
[57] W. P. Jesse and J. Sadauskis, Phys. Rev. **97**, 1668 (1955).
[58] N. Ishida, J. Kikuchi, and T. Doke, Jpn. J. Appl. Phys. **31**, 1465 (1992), and references therein.
[59] L. Onsager, Phys. Rev. **54**, 554 (1938).
[60] G. Jaffé, Ann. Phys. (Berlin) **347**, 303 (1913).
[61] H. A. Kramers, Physica (Amsterdam) **18**, 665 (1952).
[62] A. Ghosh, Ph.D. thesis, Brown University, 2005.
[63] B. Sethumadhavan, Ph.D. thesis, Brown University, 2007.
[64] D. N. McKinsey, Ph.D. thesis, Harvard University, 2002.
[65] D. N. McKinsey, C. Brome, J. Butterworth, S. Dzhosyuk, P. Huffman, C. Mattoni, J. Doyle, R. Golub, and K. Habicht, Phys. Rev. A **59**, 200 (1999).
[66] J. W. Keto, F. J. Soley, M. Stockton, and W. A. Fitzsimmons, Phys. Rev. A **10**, 872 (1974).
[67] R. Mehrotra, E. K. Mann, and A. J. Dahm, J. Low Temp. Phys. **36**, 47 (1979).
[68] D. E. Zmeev, F. Pakpour, P. M. Walmsley, A. I. Golov, W. Guo, D. N. McKinsey, G. G. Ihas, W. F. Vinen, and P. V. E. McClintock, J. Low Temp. Phys. **171**, 207 (2013).
[69] H. A. Roberts and F. L. Hereford, Phys. Rev. A **7**, 284 (1973).
[70] D. N. McKinsey, W. H. Lippincott, J. A. Nikkel, and W. G. Rellergert, Phys. Rev. Lett. **95**, 111101 (2005).
[71] G. Plante, E. Aprile, R. Budnik, B. Choi, K.-L. Giboni, L. W. Goetzke, R. F. Lang, K. E. Lim, and A. J. Melgarejo Fernandez, Phys. Rev. C **84**, 045805 (2011).
[72] C. E. Dahl, Ph.D. thesis, Princeton University, 2009.
[73] E. Aprile, K. L. Giboni, P. Majewski, K. Ni, and M. Yamashita, IEEE Trans. Nucl. Sci. **51**, 1986 (2004).
[74] P. Benetti, R. Acciarri, F. Adamo, B. Baibussinov, M. Baldoceolin, M. Belluco, F. Calaprice, E. Calligarich, M. Cambiaghi, and F. Carbonara, Astropart. Phys. **28**, 495 (2008).
[75] A. I. Bolozdynya, *Emission Detectors* (World Scientific, Singapore, 2010).
[76] C. A. N. Conde and A. J. P. L. Policarpo, Nucl. Instrum. Methods **53**, 7 (1967).
[77] A. Buzulutskov, J. Dodd, R. Galea, Y. Ju, M. Leltchouk, P. Rehak, V. Tcherniatine, W. J. Willis, A. Bondar, D. Pavlyuchenko, R. Snopkov, and Y. Tikhonov, Nucl. Instrum. Methods Phys. Res., Sect. A **548**, 487 (2005).
[78] A. F. Buzulutskov, JINST **7**, C02025 (2012).
[79] A. Breskin, R. Alon, M. Cortesi, R. Chechik, J. Miyamoto, V. Dangendorf, J. Maia, and J. M. F. Dos Santos, Nucl. Instrum. Methods Phys. Res., Sect. A **598**, 107 (2009).
[80] P. Sorensen, Phys. Rev. D **86**, 101301 (2012).
[81] A. Manalaysay, Ph.D. thesis, University of Florida, 2010.
[82] J. C. Long *et al.*, arXiv:physics/0603231.
[83] T. M. Ito, J. Phys. Conf. Ser. **69**, 012037 (2007).
[84] D. H. Beck, D. Budker, and B. K. Park (nEDM Collaboration), arXiv:1111.1273.
[85] Y. H. Huang, R. E. Lanou, H. J. Maris, G. M. Seidel, B. Sethumadhavan, and W. Yao, Astropart. Phys. **30**, 1 (2008).
[86] R. Agnese *et al.*, arXiv:1304.4279.
[87] C. F. Barnett and H. K. Reynolds, Phys. Rev. **109**, 355 (1958).
[88] P. Rudnick, Phys. Rev. **38**, 1342 (1931).
[89] P. Hvelplund and E. Horsdal Pedersen, Phys. Rev. A **9**, 2434 (1974).
[90] W. H. Cramer and J. H. Simons, J. Chem. Phys. **26**, 1272 (1957).
[91] R. Hegerberg, T. Stefansson, and M. T. Elford, J. Phys. B: At. Mol. Phys. **11**, 133 (1978).
[92] R. D. DuBois, Phys. Rev. A **39**, 4440 (1989).
[93] L. I. Pivovar, V. M. Tubaev, and M. T. Novikov, Sov. Phys. JETP **14**, 20 (1962).
[94] M. E. Rudd, T. V. Goffe, A. Itoh, and R. D. DuBois, Phys. Rev. A **32**, 829 (1985)
[95] R. D. Rivarola and R. D. Piacentini, Phys. Rev. A **20**, 1816 (1979).
[96] T. P. Grozdanov and R. K. Janev, J. Phys. B: At. Mol. Phys. **13**, 3431 (1980).

[97] M. J. Fulton and M. H. Mittleman, Proc. Phys. Soc. London **87**, 669 (1966).
[98] L. I. Pivovar, M. T. Novikov, and V. M. Tubaev, Sov. Phys. JETP **15**, 1035 (1962).
[99] G. R. Hertel and W. S. Koski, J. Chem. Phys. **40**, 3452 (1964).
[100] W. Stich, H. J. Luedde, and R. M. Dreizler, J. Phys. B: At. Mol. Phys. **18**, 1195 (1985).
[101] W. K. Wu, B. A. Huber, and K. Wiesemann, At. Data Nucl. Data Tables **40**, 57 (1988); P. Hvelplund, J. Heinemier, E. H. Pedersen, and F. R. Simpson, J. Phys. B: At. Mol. Phys. **9**, 491 (1976).
[102] H. C. Hayden and N. G. Utterback, Phys. Rev. **135**, A1575 (1964).
[103] C. F. Barnett and P. M. Stier, Phys. Rev. **109**, 385 (1958).
[104] L. J. Puckett, G. O. Taylor, and D. W. Martin, Phys. Rev. **178**, 271 (1969).
[105] R. D. DuBois, Phys. Rev. A **36**, 2585 (1987).
[106] A. C. F. Santos, W. S. Melo, M. M. SantAnna, G. M. Sigaud, and E. C. Montenegro, Phys. Rev. A **63**, 062717 (2001).
[107] M. B. Shah and H. B. Gilbody, J. Phys. B: At. Mol. Phys. **18**, 899 (1985).
[108] J. Barreto *et al.* (DAMIC Collaboration), Phys. Lett. B **711**, 264 (2012).
[109] R. Bernabei *et al.* (DAMA Collaboration), Eur. Phys. J. C **56**, 333 (2008), DAMA/LIBRA first results; as interpreted by C. Savage, G. Gelmini, P. Gondolo, and K. Freese, J. Cosmol. Astropart. Phys. 04 (2009) 010.
[110] R. Gaitskell, V. Mandic, and J. Filippini, http://dmtools.brown.edu/.